JOURNAL OF SYNCHROTRON RADIATION

ISSN 1600-5775

Impact of beryllium microstructure on the imaging and optical properties of X-ray refractive lenses

Ivan Lyatun,[a] Peter Ershov,[a] Irina Snigireva[b] and Anatoly Snigirev[a]*

[a]Immanuel Kant Baltic Federal University (IKBFU), Gaidara 6, Kaliningrad 236041, Russian Federation, and [b]European Synchrotron Radiation Facility (ESRF), 71 Avenue des Martyrs, 38043 Grenoble, France. *Correspondence e-mail: anatoly.snigirev@gmail.com

Received 19 June 2019
Accepted 19 November 2019

Edited by A. Stevenson, Australian Synchrotron, Australia

Keywords: X-ray optics; refractive lenses; beryllium microstructure; optical performance.

Beryllium is one of the most transparent materials to hard X-ray radiation and, as a direct consequence, it is the main material for the fabrication of X-ray refractive optics and instrumentation for synchrotron radiation sources and free-electron laser facilities. However, it is known that almost all beryllium currently in use is polycrystalline material. In this paper, the influence of the microstructure of different beryllium grades on the optical properties of X-ray refractive lenses is studied. The experiments were performed at the ESRF ID06 beamline in X-ray coherent transmission microscopy mode in the near- and far-fields. Two sets of refractive lenses made of beryllium O-30-H and IS-50M grades with different internal microstructure were used. It was found that both beryllium grades have a strongly inhomogeneous structure, which inevitably produces speckle patterns under coherent illumination in imaging experiments. It was shown that fine-grained beryllium O-30-H is better suited for imaging applications, whereas beryllium IS-50M with a relatively large grain microstructure is more appropriate for focusing and collimation of X-rays. A discussion on the requirements for X-ray optical materials used at the third- and fourth-generation synchrotrons is also presented.

1. Introduction

The last two decades have seen the rapid development of brilliant highly coherent beams produced by third-generation synchrotrons and free-electron lasers. New and upgraded X-ray sources provide high-energy X-ray radiation with high flux density, which leads to stricter requirements for beam conditioning and focusing systems. Compound refractive lenses (CRLs) (Snigirev *et al.*, 1996; Snigireva & Snigirev, 2006; Snigirev & Snigireva, 2008) and devices based on refractive optics, such as transfocators (Snigirev *et al.*, 2009; Vaughan *et al.*, 2011; Narikovich *et al.*, 2018, 2019), meet these requirements. Although these devices were first introduced only ∼20 years ago, refractive optics have become very popular due to their reliability, compactness and ease of use accompanied by excellent focusing and imaging performance. However, despite the successful development of refractive optics, the diffraction-limited resolution of these lenses has not yet been reached. Resolution and image quality are mostly influenced by a non-ideal lens profile, the surface roughness and the irregular optical density of the lens material. X-ray radiation is also very sensitive to cracks, inclusions, boundaries and the orientation of grains in the material. Nevertheless, manufacturers use polycrystalline materials (Be, Al, Ni, polycrystalline diamond, *etc.*) for the fabrication of X-ray refractive lenses and windows (Polikarpov *et al.*, 2016; Roth *et al.*, 2017). Polycrystalline microstructure inevitably manifests itself by introducing parasitic scattering – speckles and

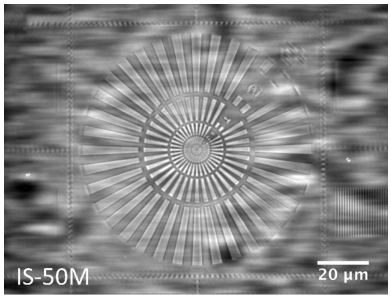

distortions that adversely affect the imaging and focusing properties of lenses. This effect is one of the limiting factors in the development of beryllium X-ray optics, not considering the non-ideal optical surface of refractive lenses. However, beryllium is now widely used as the main material for X-ray refractive optics fabrication due to its outstanding properties: the lowest X-ray absorption coefficient among any solid-state materials available under normal conditions and, at the same time, a relatively high refractive index (Lengeler *et al.*, 1999*a*; Kohn *et al.*, 2003).

We conducted extensive research on the imaging and optical properties of X-ray CRLs, which were manufactured from a wide range of different grades of metallic beryllium. This provided confirmation that the microstructure of beryllium unavoidably leads to a pronounced speckle pattern in high-energy X-ray beams during imaging experiments. In this paper, we present the results of a comparison of the X-ray optical properties of the two most promising beryllium grades used for coherent X-ray applications. The imaging properties of two-dimensional parabolic refractive lenses made of beryllium grades IS-50M and O-30-H (Materion, USA) were compared under the same conditions. In addition, we performed small-angle X-ray scattering (SAXS) studies of these beryllium grades. Finally, we propose trends in future applications of CRLs manufactured from IS-50M and O-30-H beryllium and discuss the requirements for X-ray optical materials at third- and fourth-generation synchrotron sources.

2. Beryllium material description

Due to its low atomic number and very low absorption of X-rays, beryllium is the preferred choice for the windows of X-ray tubes and synchrotron sources, where maximum beam transmission is desired. In addition, for X-ray spectroscopy studies, the sample holder and cells are usually made of beryllium, since its emitted X-rays have much lower energies ($\sim$100 eV) than X-rays from most other studied materials.

It is evident that beryllium is one of the best material for imaging applications. Therefore, extreme demands are placed on the purity of beryllium to avoid artefacts in the X-ray images. Today, most beryllium CRLs are manufactured from Be grades that are commercially available from Materion (former Brush Wellman, USA). It is known that beryllium bonds very strongly with oxygen, and all oxygen in beryllium is in the form of beryllium oxide (beryllia, BeO). Therefore, this material is resistant to air corrosion due to its thin protective BeO film which can vary from 2 to 20 nm (Yurkevich *et al.*, 2017). The concentration and the thickness of beryllia depend on the temperatures at which metallic Be is fabricated and processed (Papirov, 1969; Tomastik *et al.*, 2005). It is worth noting that beryllium oxide is the main impurity compound that decorates each Be grain and its concentration can reach up to several percent. The metal's high reactivity necessitates complex multi-stage processes to purify beryllium from oxygen. Such purification makes it possible to obtain high-quality beryllium grades with low X-ray absorption. After multiple combinations of chemical and mechanical extraction methods for beryllium metal production from ore, liquid beryllium is cast into graphite moulds, where it solidifies with large equiaxed grains (Rosenqvist, 1983; Dombrowski, 1997). To reduce the grain size and obtain the desired mechanical properties, the beryllium ingot must be processed either by the powder metallurgy process or by extensive rolling. Obviously, the methods selected for beryllium metal manufacturing and processing determine the grain size, impurity concentration, anisotropy and oxide phase concentration. Moreover, today manufacturers of X-ray optics base their choice of beryllium grades only on the mechanical properties of the material and do not consider the optical properties of beryllium. Although it has been surmised that these properties can be important (Lyatun *et al.*, 2015), a systematic study has not been conducted to quantify these effects.

Therefore, a wide range of beryllium grades from Materion (USA), Kazakhstan and Russian manufacturers have been meticulously investigated in order to study the influence of the internal microstructure on the image formation through optical elements (Semenov *et al.*, 2018; Lyatun *et al.*, 2015). However, in this paper we are focused on the comparison results and demonstration of the optical properties of the two most promising beryllium grades – O-30-H and IS-50M (Materion). These beryllium grades were chosen due to their distinctive differences in average Be grain size and beryllia content.

IS-50M beryllium grade is designed specifically for X-ray imaging applications that must be radiographically artefact-free at X-ray energy levels down to 15 keV. This beryllium grade is manufactured by hot rolling of beryllium plates in steel jackets, which allows a low concentration of BeO (0.2–0.5%) to be maintained. Unfortunately, this leads to an increase in grain size up to 100 µm and more (Roth *et al.*, 2014).

O-30-H Be grade is an optical grade of beryllium, suitable for low-scatter optical applications. This is a high density, high purity, low oxide material with good polishing characteristics. This grade is produced by machining the beryllium ingot into chips that are relatively large and not spherical. Beryllium powder is made by inert gas atomization without grinding. Beryllium metal stock is put into an induction heating crucible, melted, and poured through a nozzle as a thin liquid cylinder or sheet. High-pressure gas jets break up the liquid into fine particles; the breakup of the liquid by gas is called atomization. In beryllium atomization, oxygen is added to the atomization gas to passivate the beryllium powder surface. This prevents any rapid exothermic reaction of the fine powder with air after atomization. The oxygen concentration in the resulting fine, spherical beryllium powder is a function of the oxygen content in the melt, and surface oxidation of the molten beryllium droplets by the 1% oxygen in the atomization gas. The final oxygen content of gas-atomized beryllium is about half or less of the beryllium made using the grinding processes, but it is still higher than by rolling. The powder of O-30-H is consolidated using hot isostatic pressing, which is a diffusion bonding technique. Therefore, the size of the powder grains is below 50 µm. According to the technical data, the

O-30-H average grain size is about 15 µm and the concentration of the oxide phase is up to 0.5%.

3. Experimental results

3.1. Scanning electron microscopy

The microstructure of different beryllium grades was studied using a Zeiss Crossbeam 540 dual-beam (FIB-SEM) system in the backscattering electron regime. The electron energy was 30 keV, the working distance was around 10 mm, and the beam current was 100 nA. Fig. 1 depicts SEM images of longitudinal surface sections showing the microstructure of beryllium X-ray refractive lenses from O-30-H and IS-50M grades. Grains in the pressed beryllium powder grade O-30-H have a spherical shape and their sizes generally range from 5 to 50 µm [Fig. 1(*a*)]. It should be noted that each grain is sharply highlighted by white contrast. Moreover, the white contour generally coincides with the grain boundaries where the main impurities are concentrated. It is well known that oxygen in beryllium is mainly present as BeO and it is distributed between the grains, which is easily confirmed by surface-sensitive methods such as Auger electron and energy-dispersive X-ray spectroscopy. Since the beryllium oxide has significantly different physical and optical properties than beryllium (Table 1) (McColm, 2013; Henke *et al.*, 1993), compared with beryllium, it gives a higher contrast on SEM images. As for the IS-50M beryllium grade [Fig. 1(*b*)], it has non-spherical grains and their sizes are around 100 µm or even larger. White contrast is also observed, but the thickness of the BeO layer is thinner. All these observations are correlated to the beryllium production process and were expected. Based on the SEM images, we schematically present the internal structure of individual lenses made from these Be grades in Figs. 1(*c*) and 1(*d*). Since impurities, mostly oxygen, concentrate mainly at the grain boundaries, the defects in the internal structure of beryllium lenses can be represented as a three-dimensional BeO matrix. The size of the matrix is determined by the average grain size in the selected beryllium grade, while the thickness of the matrix wall is defined by the oxide concentration. It is easy to assume that, when a coherent wavefront passes through such a grain structure with an inhomogeneous electron density distribution (n_e), an abrupt phase discontinuity is observed at the grain/oxide film boundary (or BeO matrix). This leads to a pronounced speckle pattern formation. Such a speckle generator contains features with random high spatial frequencies, which will lead to a decrease in sensitivity to phase objects and low contrast of images in the coherent imaging mode (Falch *et al.*, 2018). In addition, undesirable small-angle X-ray scattering results in the blurring of images, reducing the effectivity and resolution of the refractive lens. Therefore, to study the impact of beryllium's internal microstructure on the optical properties of compound refractive lenses, the X-ray microscopy method was used.

Table 1
A comparison of the mechanical and optical properties of Be and BeO, where δ is the refractive index decrement and β is the absorption index of the complex refractive index $n = 1 - \delta + i\beta$.

	Material	
Property	Be	BeO
Density (g cm^{-3})	1.848	3.001
Hardness (Mohs) (MPa)	5.5	9.0
δ ($\times 10^6$ @ 12 keV)	2.37	4.16
β ($\times 10^9$ @ 12 keV)	0.37	5.44

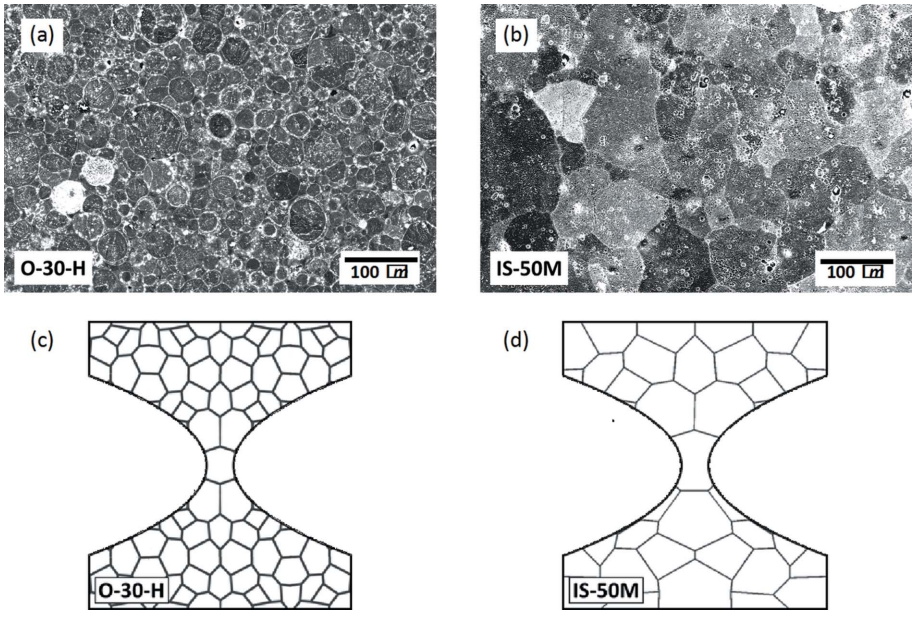

Figure 1
SEM images of beryllium microstructure of O-30-H (*a*) and IS-50M (*b*) grades. A visualization of the internal structure of O-30-H (*c*) and IS-50M (*d*) beryllium X-ray refractive lenses.

3.2. Transmission X-ray microscopy and SAXS experiments

A comparison of the X-ray optical properties of two-dimensional parabolic refractive lenses made of beryllium grades IS-50M and O-30-H was performed at the Micro-Optics Test Bench (MOTB) at the ID06 ESRF beamline (Grenoble, France). Both types of CRLs were manufactured by RXOPTICS (https://www.rxoptics.de) using the pressing technique. In the experiment, two sets of Be CRLs were used, each of which consisted of 31 individual lenses with a curvature radius of 50 µm at the apex of the parabolic profile. Since the beryllium microstructure is located inside the objective lens, let us consider the process of formation of grain images, like the propagation of the wavefront through such granular structure, separately from

the formation of the image by the objective lens. It should be noted that the average grain size in the grades O-30-H and IS-50M differs by almost ten times, which leads to the fact that the Fresnel numbers F_n [$F_n = (d/2)^2/\lambda L_2$, where d is the average grain size, λ is the wavelength and L_2 is the lens–detector distance] differ by two orders of magnitude. Therefore, for this experiment, it would be reasonable to use two distances between the lens and the detector: the relatively short and rather long so-called near- and far-fields.

To study the effect of the microstructure of beryllium lenses in the near-field, we performed X-ray microscopy at 12.0 keV photon energy (λ = 1.033 Å) in a demagnification setup, shown in Fig. 2(*a*). The desired energy was selected by using a double-crystal Si monochromator with (111) orientation. Higher harmonics were suppressed by detuning the second crystal of the Si monochromator from the Bragg condition by 20% of the angular width range of Si reflection. As a test object, a copper transmission electron microscopy square grid with a period of 63.5 µm (400 lines inch^{-1}) was used. The Cu grid was placed at a distance of 1.04 m (L_1) in front of the refractive lenses. X-ray images were recorded using a high-resolution X-ray CCD camera with a 0.645 µm pixel size, which was located at a distance of 0.52 m (L_2) behind the lenses. The overall magnification factor for the tested X-ray microscopy setup was 0.5×.

Figs. 2(*b*) and 2(*c*) show images of a copper grid, which were obtained using two sets of beryllium CRLs of different grades. The influence of the grains in the beryllium grade O-30-H on the image formation is less pronounced than in the IS-50M grade. In this layout, the visualization of beryllium grains in the lens material was performed in the near-field. The Fresnel distance for 15 µm grains is around 0.5 m, so at the position of the detector the image of the grain is almost blurred; while for 100 µm grains, the Fresnel distance is around 24 m and the grains are sharply visible [Fig. 2(*c*)]. The quantitative evaluation of the images was carried out on the basis of calculating the contrast-to-noise ratio (CNR) for both images in accordance with formula (1) (Song *et al.*, 2004),

$$\mathrm{CNR} = \frac{I_\mathrm{b} - I_\mathrm{s}}{\left[\left(\sigma_\mathrm{b}^2 + \sigma_\mathrm{s}^2\right)/2\right]^{1/2}}. \qquad (1)$$

The horizontal and vertical profiles of the intensity distribution [Figs. 2(*d*) and 2(*e*)] were used to obtain the values of the signal (I_s) and background (I_b) intensity for calculating the root-mean-square deviations of intensity σ_s and σ_b for each signal-to-noise 'step'. We calculated the averaged CNR for each image, using a series of horizontal and vertical linear profiles of the intensity distribution. Image quality assessments show that the test object image obtained using the IS-50M grade beryllium lenses (with an average Be grain size of approximately 100 µm) has a lower contrast-to-noise ratio (CNR = 5.9) and a higher noise level. The image in Fig. 2(*b*), obtained using O-30-H grade lenses (average Be grain size of 15 µm), is characterized by a higher contrast-to-noise ratio (CNR = 9.7) and better image quality.

To study the influence of the structure of beryllium lenses in the far-field, we implemented a scheme for magnifying transmission X-ray microscopy, which is shown in Fig. 3(*a*). As in the previous experiment, the same sets of Be refractive lenses were used as an objective lens. A 0.5 µm-thick Ta Siemens star test object was placed at a distance of L_1 = 0.59 m in front of the objective. A high-resolution CCD camera was located at a distance of L_2 = 6.44 m after the CRLs. Under this arrangement, we achieved a magnification factor of ∼11×. X-ray

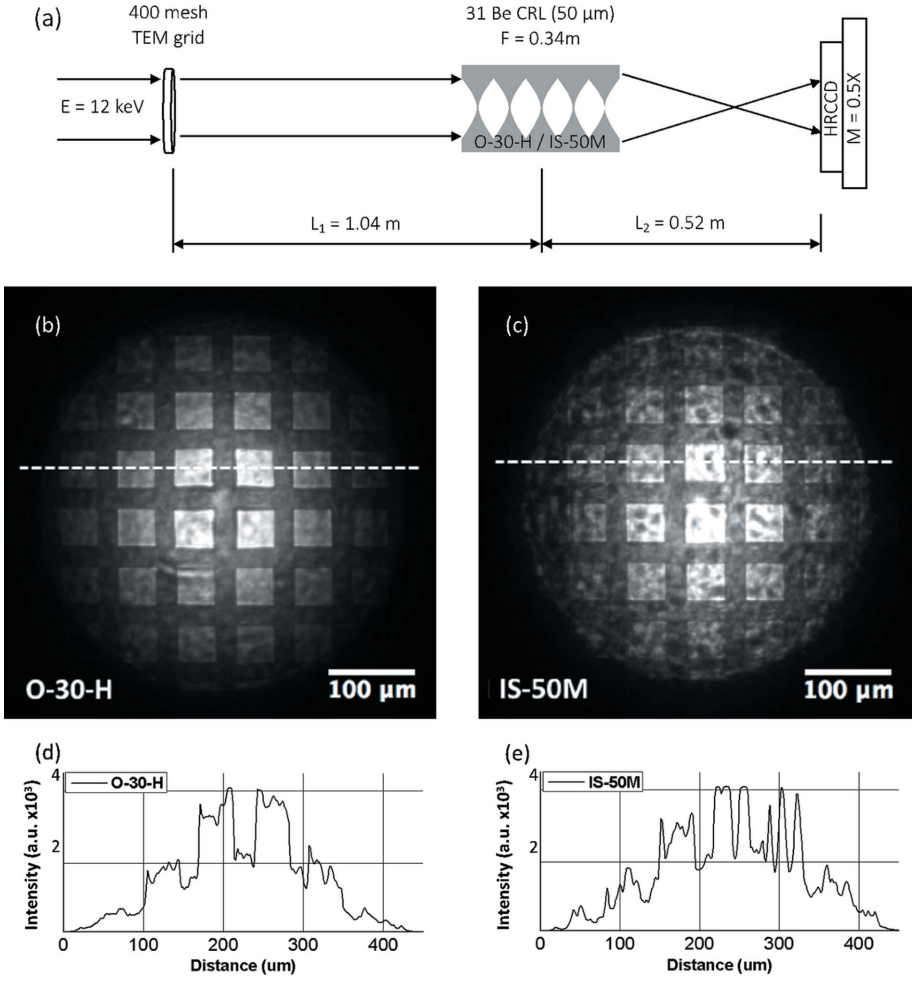

Figure 2
Experimental layout of X-ray microscopy with two sets of IS-50M and O-30-H refractive lenses (*a*). Images of the test structure in the near-field, obtained using beryllium CRLs grades O-30-H (*b*) and IS-50M (*c*). Intensity distribution profiles measured along the line marked on the images of the test structure obtained using CRLs of grades O-30-H (*c*) and IS-50M (*d*).

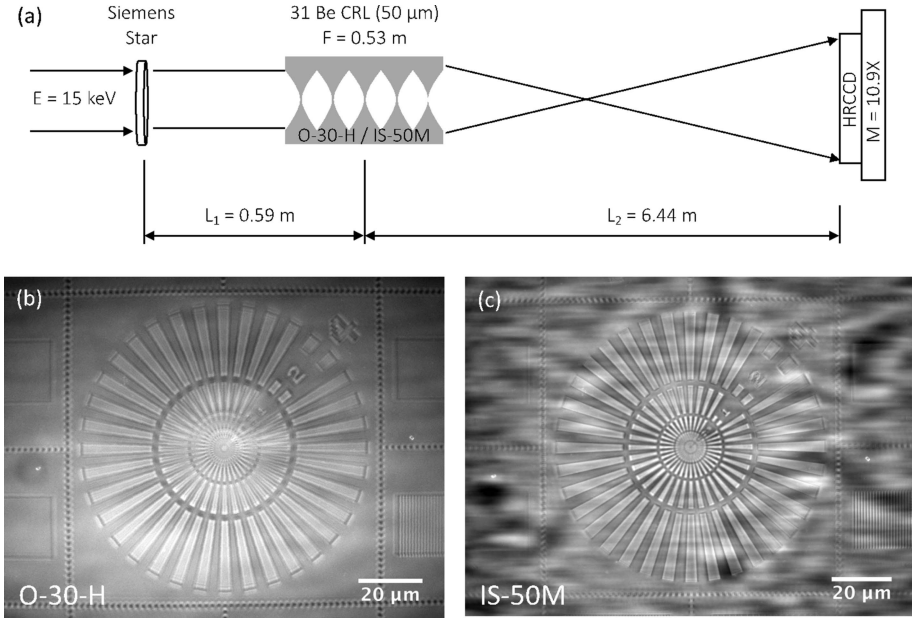

Figure 3
Far-field X-ray microscopy experimental layout (*a*). X-ray images of the Siemens star test structure, obtained using beryllium CRLs grades O-30-H (*b*) and IS-50M (*c*).

images of the test object obtained at 15.0 keV are shown in Figs. 3(*b*) and 3(*c*). The image obtained with the O-30-H lens is significantly different for the better due to fine blurred small internal beryllium microstructure [Fig. 3(*b*)]. The image in Fig. 3(*c*) is characterized by a strong non-uniform background, and the speckle pattern from grains in the IS-50M lenses is still visible. The size of the speckles, a statistical average of the distance between adjacent regions of maximum and minimum brightness, can be estimated as $D \simeq 1.2\lambda L_2/d$ (Dainty, 2013), and the speckle size is $\sim$80 μm and $\sim$8 μm for beryllium grades O-30-H and IS-50M, respectively. Relatively large beryllium grains lead to small speckles, while small beryllium grains lead to larger ones. These data on the size of the speckles are in good agreement with the size of the speckles obtained in far-field X-ray microscopy mode, as shown in Figs. 3(*b*) and 3(*c*).

In order to improve image quality and increase the CNR value in coherent imaging experiments, it is necessary to enhance the image contrast and minimize the σ_s and σ_b values. Image contrast C can be calculated as follows,

$$C = \frac{I_b - I_s}{I_b + I_s}. \qquad (2)$$

However, in the case of low absorbing objects, the quality of the images in the hard X-ray range can be improved by reducing the σ value. It is known that the value of the root-mean-square deviation (σ) directly depends on undesirable variations in the electron density n_e in the X-ray optics materials, and this is especially noticeable in beryllium.

One of the methods to reduce the parasitic effect of microstructured optical elements is the use of monocrystalline materials for the manufacture of X-ray refractive optics and windows. However, if the condition for X-ray diffraction can be fulfilled for one or several individual single-crystal refractive lenses, then the intensity of transmitted X-radiation will decrease significantly (Polikarpov *et al.*, 2018). Another way to eliminate the speckle pattern produced by optical elements is by the use of X-ray homogeneous and fully amorphous materials. It was reported that Be foil, grown by plasma vapour deposition, does not give a speckle pattern with coherent X-rays (Goto *et al.*, 2007). However, this method does not permit the production of beryllium foils with a thickness of more than 500 μm, which is necessary for manufacturing CRLs. It is worth noting that currently there are no data on the radiation stability and toxicity of completely amorphous beryllium or its compounds when used in the laboratory and synchrotron beamlines. In this regard, the beryllium speckle patterns in X-ray microscopy experiments can be suppressed by using polycrystalline materials with reduced grain size. The angular range of the speckle pattern formation can be defined as $\sim\lambda/d$, where d is the average beryllium grain size. It is also known that the typical angular size of the detector in X-ray microscopy experiments is 50–500 μrad (Lengeler *et al.*, 1999*a*,*b*; Bosak *et al.*, 2010). Therefore, reducing the average beryllium grain size to $\leq$100 nm will significantly increase the angular range of the speckle pattern formation. It will also reduce the parasitic σ value for images formed in the coherent imaging mode with high-resolution in the ultra-small angular range.

To confirm the revealed dependence of the influence of the grain size on the image quality and visibility of a speckle pattern, the angular dependence of X-ray scattering from IS-50M and O-30-H beryllium grades was investigated. Experimental SAXS data were obtained at the ID06 ESRF beamline using monochromatic X-ray radiation with an energy of 12 keV (wavelength λ = 1.033 Å). To reduce the parasitic scattering, which determines the minimum observable scattering angle, three slit sets were used, and guard slits (S5) of 200 μm × 200 μm size limited the beam size on the sample. The distance from the sample to the detector was 5.83 m. For these experiments, one lens from each set (IS-50M and O-30-H) was chosen. A 1 mm-thick part of the lens, that was far from the physical aperture, was irradiated. Small-angle scattering patterns were acquired using a Photonic Science 2×2k sCMOS camera with a pixel size of 6.5 μm. Fig. 4 shows the experimentally measured scattering intensity for ultra-low angles in the range 30–200 μrad for the two grades of beryllium. Obviously, the classical SAXS technique does not allow us to fully characterize the influence of microstructure on lens imaging properties since it is impossible to measure scattering at angles smaller than the angular dimensions of the beamstop. However, it is clearly seen that beryllium grade O-30-H makes

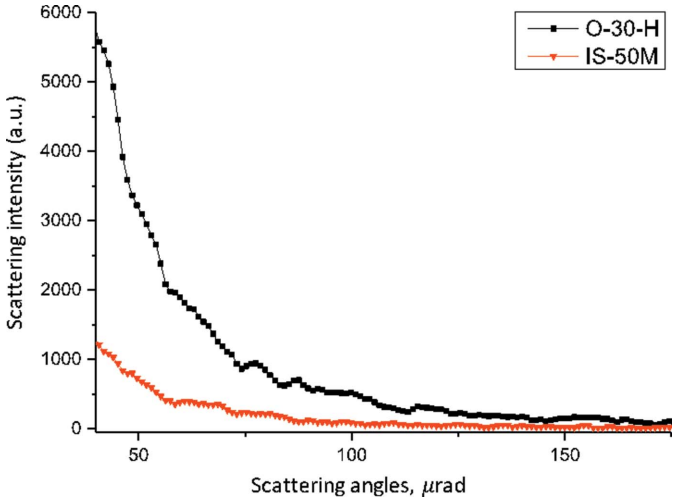

Figure 4
Small-angle X-ray scattering curves for IS-50M and O-30-H beryllium grades, obtained at X-radiation energy of 12 keV.

a greater contribution to the observed scattering than beryllium IS-50M; this is especially noticeable for angles from 30 to 100 μrad. These data are completely consistent with the results of grain size estimation using scanning electron microscopy. Small grains with a thick layer of beryllium oxide in beryllium type O-30-H produce a scattering pattern in a wider angular range and with greater intensity; whereas large grains with a thin film of beryllium oxide in beryllium grade IS-50M produce a scattering pattern in a smaller angular range, and its intensity is lower.

4. Discussion and conclusions

This work demonstrates for the first time the influence of the internal microstructure of beryllium on the optical properties of beryllium refractive lenses in a coherent X-ray microscopy mode. It was experimentally shown that the formation of speckle structure is caused by optical inhomogeneities inside beryllium optical elements. It was revealed that the internal beryllium microstructure is a developed three-dimensional matrix of beryllium oxide, the optical properties of which differ significantly from the Be grain. Thus, when the coherent wavefront passes through such a grain structure, the BeO matrix forms a speckle pattern behind beryllium optical elements. The relatively large beryllium microstructure (grain size 10–100 μm) manifests itself quite brightly in the near-field (at short imaging distances). This leads to a deterioration of the contrast and image quality due to the appearance of the noise signal. Since images obtained using IS-50M grade beryllium lenses have lower image quality, they are therefore less suitable for imaging phase objects in the near-field as compared with O-30-H grade lenses. In the far-field, the influence of large beryllium grains in IS-50M lenses on the image quality is less pronounced, but the non-uniform background and speckle pattern are still visible.

The incomparable quality of images produced using CRLs of different grades (Figs. 2 and 3) is due to differences in the sizes of beryllium grains. It was shown that the average beryllium grain size of the O-30-H grade is one-tenth of the grain size in the IS-50M grade. This leads to an almost complete blurring of the 'image' of the grain and a smaller contribution of parasitic diffuse X-rays scattered to the ultra-small viewing angles. Thus, on the one hand, relatively small beryllium microstructure in O-30-H lenses allows obtaining X-ray images in the far-field without an undesirable speckle pattern with a spatial resolution up to 100 nm. On the other hand, the 'wide-angle' scattering on grains of 15 μm in O-30-H lenses causes additional loss of intensity from 20% to 40% already at distances from 0.5 m to 14.5 m, compared with lenses of the IS-50M grade.

We also conducted a study of the focusing properties of CRLs from these two grades (the result will be presented in our next paper) and it turned out that no change was found in the size and shape of the focal spot for the two sets of lenses. Thus, IS-50M grade beryllium lenses will be more effective for hard X-ray focusing, transport and collimation applications, since a lower concentration of beryllium oxide in this grade will minimize X-ray scattering and absorption losses.

Reducing the average size of beryllium grains in a lens material is crucial for their implementation in coherent imaging applications. Consequently, the use of beryllium grades with a grain size of less than 100 nm (nanoberyllium grade) in the manufacturing of refractive lenses and windows will improve the image quality by minimizing the contribution of the material microstructure to the small-angle scattering in the near- and far-fields. It should be noted that reducing the grain size will certainly lead to a noticeable increase in BeO concentration, which is expected to cause significant loss of intensity due to X-ray scattering and absorption, as well as complicating the machining of this beryllium grade and the manufacture of refractive optics. Another alternative way to effectively suppress the speckle pattern of the lens is based on the use of high-porosity beryllium, the so-called 'speckle suppressor' (Goikhman *et al.*, 2015). However, this approach reduces the sensitivity of X-ray microscopes for imaging weakly absorbing objects with a fine structure. Thus, for novel diffraction-limited X-ray sources, new optics and instrumentations without an internal microstructure are required, *i.e.* made from completely amorphous and optically homogeneous materials (Petrov *et al.*, 2017; Roth *et al.*, 2017).

In addition, it should be noted that the sensitivity of coherent X-ray microscopy to the imperfections of the lens material can be extremely useful for diagnosing the quality of optics, as was done with the use of X-ray diffraction for growing perfect single-crystal silicon. We are confident that X-ray coherent microscopy can be a powerful tool for improving the quality of optical materials, which can later be used for imaging applications.

Acknowledgements

The authors are very grateful to C. Detlefs, P. Wattecamps, M. Lyubomirskiy and M. Polikarpov for their assistance during the experiments at the ID06 ESRF beamline. The

authors thank V. Savin, A. Sinitsyn, D. Zverev and E. Clementyev for their helpful discussions.

Funding information

The following funding is acknowledged: This research (except for SEM studies) was supported by Russian Science Foundation (Project No. 19-72-30009); The SEM studies were supported by the Russian Academic Excellence Project at the Immanuel Kant Baltic Federal University.

References

Bosak, A., Snigireva, I., Napolskii, K. S. & Snigirev, A. (2010). *Adv. Mater.* **22**, 3256–3259.

Dainty, J. C. (2013). *Laser Speckle and Related Phenomena.* Springer Science & Business Media.

Dombrowski, D. E. (1997). *Fusion Eng. Des.* **37**, 229–242.

Falch, K. V., Lyubomirsky, M., Casari, D., Snigirev, A., Snigireva, I., Detlefs, C., Michiel, M. D., Lyatun, I. & Mathiesen, R. H. (2018). *Ultramicroscopy*, **184**, 267–273.

Goikhman, A., Lyatun, I., Ershov, P., Snigireva, I., Wojda, P., Gorlevsky, V., Semenov, A., Sheverdyaev, M., Koletskiy, V. & Snigirev, A. (2015). *J. Synchrotron Rad.* **22**, 796–800.

Goto, S., Yabashi, M., Tamasaku, K. & Ishikawa, T. (2007). *AIP Conf. Proc.* **879**, 1057–1060.

Henke, B. L., Gullikson, E. M. & Davis, J. C. (1993). *At. Data Nucl. Data Tables*, **54**, 181–342.

Kohn, V., Snigireva, I. & Snigirev, A. (2003). *Opt. Commun.* **216**, 247–260.

Lengeler, B., Schroer, C. G., Richwin, M., Tümmler, J., Drakopoulos, M., Snigirev, A. & Snigireva, I. (1999). *Appl. Phys. Lett.* **74**, 3924–3926.

Lengeler, B., Schroer, C., Tümmler, J., Benner, B., Richwin, M., Snigirev, A., Snigireva, I. & Drakopoulos, M. (1999*a*). *J. Synchrotron Rad.* **6**, 1153–1167.

Lyatun, I. I., Goikhman, A. Y., Ershov, P. A., Snigireva, I. I. & Snigirev, A. A. (2015). *J. Synch. Investig.* **9**, 446–450.

McColm, I. J. (2013). *Dictionary of Ceramic Science and Engineering.* Springer Science & Business Media.

Narikovich, A., Baranikov, A., Ershov, P., Klimova, N., Lushnikov, A., Lyatun, I., Panormov, I., Polikarpov, M., Sinitsyn, A., Zverev, D., Snigireva, I. & Snigirev, A. (2018). *Microsc. Microanal.* **24**, 294–295.

Narikovich, A., Polikarpov, M., Barannikov, A., Klimova, N., Lushnikov, A., Lyatun, I., Bourenkov, G., Zverev, D., Panormov, I., Sinitsyn, A., Snigireva, I. & Snigirev, A. (2019). *J. Synchrotron Rad.* **26**, 1208–1212.

Papirov, I. I. (1969). FTD-HT-23-110-69. Foreign Technology Division Wright-Patterson, AFB Ohio, USA.

Petrov, A. K., Bessonov, V. O., Abrashitova, K. A., Kokareva, N. G., Safronov, K. R., Barannikov, A. A., Ershov, P. A., Klimova, N. B., Lyatun, I. I., Yunkin, V. A., Polikarpov, M., Snigireva, I., Fedyanin, A. A. & Snigirev, A. (2017). *Opt. Express*, **25**, 14173–14181.

Polikarpov, M., Emerich, H., Klimova, N., Snigireva, I., Savin, V. & Snigirev, A. (2018). *Phys. Status Solidi B*, **255**, 1700229.

Polikarpov, M., Kononenko, T. V., Ralchenko, V. G., Ashkinazi, E. E., Konov, V. I., Snigireva, I., Ershov, P., Kuznetsov, S., Yunkin, V., Polikarpov, V. M. & Snigirev, A. (2016). *Proc. SPIE*, **9963**, 99630Q.

Rosenqvist, T. (1983). *Principles of Extractive Metallurgy*, 2nd ed. McGraw-Hill.

Roth, T., Alianelli, L., Lengeler, D., Snigirev, A. & Seiboth, F. (2017). *MRS Bull.* **42**, 430–436.

Roth, T., Helfen, L., Hallmann, J., Samoylova, L., Kwaśniewski, P., Lengeler, B. & Madsen, A. (2014). *Proc. SPIE*, **9207**, 920702.

Semenov, A. A., Volkov, V. V., Zabrodin, A. V., Gorlevskii, V. V., Sheverdyaev, M. S., Lizunov, A. V., Brylev, D. A., Anikin, A. S., Demin, A. V., Nebera, A. L., Morozov, I. A., Lesina, I. G., Kozlova, E. V., Klykov, S. S., Kupriyanov, I. B., Zhidelev, A. I., Asadchikov, V. E., Buzmakov, A. V., Roshchin, B. S., Dadinova, L. A., Chekrygina, D. I., Amarantov, S. V., Zhigalina, O. M., Khmelenin, D. N., Senin, R. A., Veligzhanin, A. A. & Aleksandrov, P. A. (2018). *Crystallogr. Rep.* **63**, 874–882.

Snigirev, A., Kohn, V., Snigireva, I. & Lengeler, B. (1996). *Nature*, **384**, 49–51.

Snigirev, A. & Snigireva, I. (2008). *C. R. Phys.* **9**, 507–516.

Snigirev, A., Snigireva, I., Vaughan, G., Wright, J., Rossat, M., Bytchkov, A. & Curfs, C. (2009). *J. Phys. Conf. Ser.* **186**, 012073.

Snigireva, I. & Snigirev, A. (2006). *J. Environ. Monit.* **8**, 33–42.

Song, X., Pogue, B. W., Jiang, S., Doyley, M. M., Dehghani, H., Tosteson, T. D. & Paulsen, K. D. (2004). *Appl. Opt.* **43**, 1053–1062.

Tomastik, C., Werner, W. & Störi, H. (2005). *Nucl. Fusion*, **45**, 1061–1065.

Vaughan, G. B. M., Wright, J. P., Bytchkov, A., Rossat, M., Gleyzolle, H., Snigireva, I. & Snigirev, A. (2011). *J. Synchrotron Rad.* **18**, 125–133.

Yurkevich, O., Maksimova, K., Goikhman, A., Grunin, A., Prokopovich, P., Tyurin, A., Medvedskaya, P., Lyatun, I., Snigireva, I. & Snigirev, A. (2017). *J. Synchrotron Rad.* **24**, 775–780.